

## Prediction of the transmission through thin-film waveguides for X-ray microscopy

Werner Jark\* and Silvia Di Fonzo

Sincrotrone Trieste, SS 14 km 163.5 in Area Science Park,  
I-34012 Basovizza (TS), Italy.  
E-mail: werner.jark@elettra.trieste.it

Thin-film slab waveguides can confine incident X-ray beams in one direction in guiding layers as thin as 10 nm. Consequently they can provide attractive beam dimensions for microscopy purposes. This report presents a simple model and analytical equations for the transmission calculation, which provide results consistent with the rigorous calculations based on recursion techniques. By using these results the waveguide transmission can be compared directly with other microscopy objectives. Ideally X-ray waveguides can filter the spatially coherent content out of an incident radiation beam with an efficiency of 1. The transmissions measured for state-of-the-art one- and two-dimensional waveguides are found to correspond to experimental efficiencies of 0.5 for each confinement direction. Waveguides with thinner guiding layers cannot be used efficiently in highly collimated beams; instead the beam divergence in unfocused beamlines at state-of-the-art synchrotron radiation sources may eventually have to be increased to the larger angular acceptance of these waveguides by use of other focusing optics.

**Keywords:** X-ray optics; X-ray microscopy; X-ray microbeams; spatial coherence; waveguides.

### 1. Introduction

Long undulators in third-generation synchrotron radiation sources and in future free-electron lasers (Andruszkow *et al.*, 2000) will concentrate the emitted radiation into very narrow emission cones. Consequently one can consider the creation of a still intense and significantly demagnified image of the source with optical components of given focal lengths at increasingly large source distances. Ultimately this image size will be limited to the diffraction-limited spot size for a particular focusing objective. With this future perspective, discussions on the smallest possible spot size behind an optical component began. Bergemann *et al.* (2003) showed that an X-ray beam cannot be further focused in a tapered double-plate waveguide when the plate distance  $W$  falls below

$$W = \lambda/2\varphi_c. \quad (1)$$

Here  $\lambda$  is the wavelength and  $\varphi_c$  is the critical angle for the material of the plates.

In the hard X-ray range the refractive index  $n$  of a material is usually written as  $n = 1 - \delta - i\beta$ , where  $\delta$  and  $\beta$  are small compared with unity and are related to the number of atoms per unit volume  $N_e$  by (Henke *et al.*, 1993)

$$\delta = \frac{r_e \lambda^2 N_e f_1}{2\pi}, \quad \beta = \frac{r_e \lambda^2 N_e f_2}{2\pi}. \quad (2)$$

Here  $f_1$  and  $f_2$  are the atomic scattering factors, which are tabulated by Henke *et al.* (1993) and Chantler *et al.* (2003), and  $r_e = 2.818 \times 10^{-15}$  m is the classical electron radius. The critical angle can then be obtained from

$$\varphi_c = (2\delta)^{1/2}, \quad (3)$$

and, as  $f_1$  is constant for a given material in the hard X-ray range,  $W$  is a constant in this range. For gold-coated plates,  $W = 8$  nm. Bergemann *et al.* (2003) then argue that this number is the natural lower limit for the smallest spot size to which X-rays can be focused by diffraction, for example also in a Fresnel zone plate.

Obviously the same limit also applies for slab waveguides with a low- $Z$  guiding layer. Indeed a beam originating from the termination of a slab waveguide with a guiding layer thickness as small as 10.4 nm was detected by Pfeiffer (1999). Spot sizes of this order have not been detected as yet by any other means. The next-closest spot size of 20 nm is reported by Chao *et al.* (2003) for Fresnel zone plates operated in the soft X-ray range with a photon energy of  $E = 600$  eV ( $\lambda = 2.07$  nm). In this case the observed spot size is actually the diffraction limit of Fresnel zone plates, which is given by the width of the outermost opaque zone (Schmahl & Rudolph, 1969; Attwood, 1999). In this case the reported number is not the ultimate natural limit, but is imposed by the present manufacturing technology. State-of-the-art Fresnel zone plates for hard X-rays still have larger zone widths (Di Fabrizio *et al.*, 1999) and thus provide larger spot sizes of the order of 80–90 nm (Yun *et al.*, 1999). Spot sizes in the same 80–90 nm range have also been obtained by Hignette (2003) by reflecting crossed KB mirror pairs (Kirkpatrick & Baez, 1948), while compound refractive lenses (CRLs) (Snigirev *et al.*, 1996) recently provided 210 nm in one direction (Schroer *et al.*, 2003). Smaller numbers are reported by Pfeiffer *et al.* (2002) for the first two-dimensional waveguides of 33 nm  $\times$  66 nm, and for multibounce capillaries providing a beam diameter of 50 nm (Bilderback *et al.*, 1994). Note that the beam compression in waveguides in one direction (Spiller & Segmüller, 1974; Feng *et al.*, 1995; Lagomarsino *et al.*, 1996) can now routinely provide beam sizes of the order of 35 nm (Di Fonzo *et al.*, 2000; Jark *et al.*, 2001), while a value of 26 nm is reported by Zwanenburg *et al.* (2000) for a tapered air-gap waveguide.

Fresnel zone plates, mirrors and CRLs fall into the categories of diffracting, reflecting and refracting objectives, which are also used in the visible range for imaging and microscopy purposes. Waveguides and capillaries are beam-compressing devices, which have no equivalent for microbeam production in the visible. Now Fresnel zone plates, mirrors and CRLs have predictable properties for the component aperture and transmission (Attwood, 1999; Born & Wolf, 1980; Lengeler *et al.*, 1999), and the experimental performance of state-of-the-art objects is always rather close to the prediction. Consequently the performance of these objectives can readily be compared. For X-ray waveguides the derivation of the parameters that can be used for this comparison has not yet been made. Consequently experimentally determined transmission efficiencies for state-of-the-art real objects are not yet available. This report will address both problems, and will thus create a first basis that will allow comparison of the X-ray waveguide performance with that of the other objectives for both aspects, the predicted performance and the experimentally determined one.

### 2. Theoretical considerations

This study assumes a monochromatic incident X-ray beam with a bandwidth  $\Delta E/E < 10^{-3}$  as is mostly used in experimental set-ups at synchrotron radiation sources. This was found to be narrower than could be accepted in X-ray waveguides (Cedola *et al.*, 1998). Note that a similar spectral resolution is needed in order to obtain the diffraction-limited spot size behind chromatic Fresnel zone plates. On the other hand, achromatic mirrors do not need a monochromatic beam, while chromatic CRLs can focus the incident radiation with a larger bandwidth (Jark, 2004).

As indicated in Fig. 1, the beam compression in X-ray waveguides is the result of constructive beam interference of the incident wavefield in the guiding layer. Consequently the phase-space acceptance of such an object is limited to the phase-space volume occupied by the spatially coherent part of the incident radiation. Indeed, the beam exiting from the waveguide terminal was found to be highly spatially coherent even in an incident incoherent beam (Feng *et al.*, 1995; Jark *et al.*, 1996). Consequently the waveguide can be considered as a filter for the spatially coherent part of the incident radiation. The consequence of this for the spatial resolution in diffraction experiments is discussed by De Caro *et al.* (2003).

If one assumes the radiation beam to be represented by Gaussian distribution functions for its spatial and its angular extent, then the spatially coherent part covers a phase-space volume given by (Attwood, 1999)

$$A\Delta\varphi = \lambda/4\pi. \quad (4)$$

In this case  $A$  and  $\Delta\varphi$  are the standard deviations for the size and the angular extent. For practical purposes it is more convenient to use full width at half-maximum (FWHM) properties, *i.e.*  $A_{\text{FWHM}} = 2.35A$  and  $\Delta\varphi_{\text{FWHM}} = 2.35\Delta\varphi$ , which each include 76% of the photon flux. This leads to

$$A_{\text{FWHM}}\Delta\varphi_{\text{FWHM}} = 0.44\lambda. \quad (5)$$

This phase-space volume in the FWHM sense will be used in order to derive here the spatial beam acceptance and the related angular acceptance of X-ray waveguides. Note that any optical component can provide the diffraction-limited spot size only if illuminated with spatially coherent radiation as given by (2). X-ray waveguides have the special property that they will not appreciably transmit spatially incoherent radiation, while other optical components can.

As shown in Fig. 1, an X-ray waveguide is a thin-film system. Consequently the electric field progression through this film system can be calculated rigorously by use of the formalism introduced by Parratt (1954). In principle this would allow the direct calculation of,

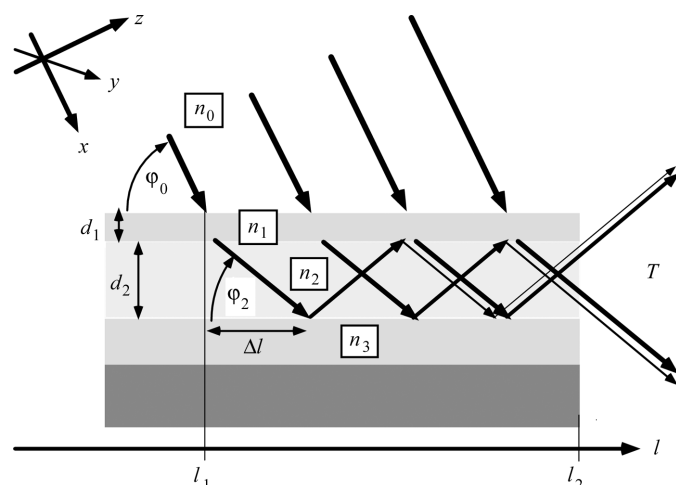


**Figure 1**

Schematic representation of a thin-film waveguide with refractive indexes  $n_1$ ,  $n_2$  and  $n_3$  for the cover layer, the core and the underlayer, respectively. The environment has  $n_0 = 1$ .  $\varphi_0$  and  $\varphi_2$  are the angles of grazing incidence onto the waveguide surface and onto the internal interfaces, respectively.  $d_1$  and  $d_2$  are the thickness for the cover and the guiding layer and  $\Delta l$  is the longitudinal beam advance between two bounces in the coordinate system of the waveguide, where  $l$  is the coordinate along the beam footprint, which extends from  $l_1$  to  $l_2$ . Arrows of different thickness approximately indicate the beam attenuation during the travelling of waves coupled earlier into the waveguide. Note that the angles and vertical dimensions are exaggerated for clarity.

for example, the angular acceptance for a given waveguide structure. However, as this rigorous approach is based on recursion techniques, one cannot immediately predict the dependence of a parameter on, for example, the guiding-layer thickness or on photon energy. Consequently, for the latter purpose the present report will present a simpler plausible model. It provides the principle parameters in analytical expressions, which agree with the rigorous calculations. Note that the beam coupling into tunable-air-gap waveguides (Zwanenburg *et al.*, 1999), whether they work with parallel plates or in the tapered version (Zwanenburg *et al.*, 2000), is made differently, and thus the present considerations cannot be applied in this case. The problems related to the efficient coupling of the incident radiation into such waveguides are discussed by Bongaerts *et al.* (2002).

## 2.1. Basic geometrical waveguide relations

In general, if the refractive indices of a layer system, as presented in Fig. 1, fulfill the condition  $n_2 > n_1 \geq n_3$  (Marcuse, 1991), electromagnetic modes (*i.e.* waves travelling in the thin film parallel to the surface) can be excited in the core layer with index 2. For X-rays, which have positive  $\delta$ , the largest refractive index  $n$  is provided by the material with the smallest  $\delta$ . Consequently, X-ray mode excitation is possible in the layer with the smallest electron density ( $N_e f_1$ ), which is also usually the less absorbing one.

As shown in Fig. 1, the incident intensity can be coupled through a thin enough cover layer directly to the permitted modes in the core layer (Spiller & Segmüller, 1974). This gives rise to resonant beam coupling. The discussion will here be restricted to the fundamental guided mode and to symmetric waveguides with  $n_1 = n_3$ . Furthermore, only the situation of maximum internal intensity enhancement far beyond the incident intensity is considered. This requires for any guiding-layer thickness  $d_2$  a specific cover-layer thickness  $d_1$ , which depends on the materials involved and on the photon energy (Lagomarsino *et al.*, 2002). For the latter discussed waveguides one has within their permitted operation range always  $d_1 < d_2$  and  $d_1 < 10$  nm (Di Fonzo *et al.*, 2000; Jark *et al.*, 2001; Pfeiffer *et al.*, 2002).  $d_1$  needs to be increased on top of thinner cores, for the efficient excitation of higher-order modes and for the operation of a given  $d_2$  at higher photon energies (smaller wavelengths).

In the case of maximum internal intensity enhancement the fundamental guided mode has its antinode almost in the center of the guiding layer and has its two nodes in the vicinity of the top surface and in the vicinity of the interface with the absorbing underlayer. Then the effective resonator thickness is  $D_{\text{eff}} = d_1 + d_2$  and the mode excitation condition for an incident X-ray beam of wavelength  $\lambda$  is given by

$$2D_{\text{eff}} \sin \varphi_2 = \lambda, \quad (6)$$

where  $\varphi_2$  is the angle of grazing incidence with respect to the internal interfaces. The FWHM beam size of the radiation exiting from the termination is then  $D_{\text{eff}}/2$ .

Under the present conditions the angles are small and thus the refraction at the interfaces can be obtained *via*

$$\varphi_0 = (\varphi_2^2 + \varphi_{c,2}^2)^{1/2}. \quad (7)$$

The guiding condition  $n_2 > n_1$  corresponds to  $\varphi_{c,1} > \varphi_{c,2}$ . On the other hand, from (7) one finds  $\varphi_0 > \varphi_{c,2}$  while we need  $\varphi_0 < \varphi_{c,1}$ . Consequently for the mode excitation the incident wavefield is tunneling through the cover layer. For the limiting case,  $\varphi_0 = \varphi_{c,1}$ , and by use of (7) and (6) one finds for  $\delta_1 \gg \delta_2$  the lower waveguide thickness limit as already given in (1).

## 2.2. Spatial and angular acceptance of X-ray waveguides

**2.2.1. One-dimensional slab waveguides.** It is the waveguide spatial acceptance which can be derived readily from plausible arguments. For simplicity we will ignore the fact that the waveguide transmission function is not symmetric with respect to the vertical direction. Instead the spatial acceptance will be taken in the FWHM sense, *i.e.* as the window size, which accepts 76% of the ultimately transmittable flux. The related aperture size can be derived from the effective aperture of the optical component, which is the component transmission function  $t(z)$  integrated over its geometrical aperture  $\{z_1, z_2\}$ ,

$$A_{\text{eff}} = \int_{z_1}^{z_2} t(z) dz. \quad (8)$$

In other words, the effective aperture is the aperture of a perfectly transparent optical system that provides the same output photon flux as our optical component positioned behind the geometrical aperture  $\{z_1, z_2\}$  (Lengeler *et al.*, 1999). The effective and geometrical aperture will be identical only for perfectly transparent optical systems, while the effective aperture is usually smaller than the geometrical aperture.

In the present geometry, the effective aperture and effective footprint size  $l_{\text{eff}}$  are related *via*  $A_{\text{eff}} = \varphi_0 l_{\text{eff}}$ . Then we can substitute  $t(z) = \varphi_0 t(l)$ , where  $l$  is the distance of an impinging ray from the waveguide exit ( $l_2 = 0$ ), and consequently the effective aperture corresponding to the ultimately possible output photon flux is obtained from

$$A_{\text{eff}} = \varphi_0 l_{\text{eff}} = \varphi_0 \int_{l_1=-\infty}^{l_2=0} t(l) dl. \quad (9)$$

Along the footprint the guided wave will be attenuated because of absorption and, in the  $n$  reflection, processes at the two interfaces (1,2) and (2,3). In the symmetric waveguides the interface reflectivity fulfils  $R_{1,2} = R_{2,3} = R$ , and  $R$  is calculated from the complex interface reflection coefficient  $\tilde{R}_{1,2}$  *via*  $R = \tilde{R}_{1,2} \tilde{R}_{1,2}^*$ , where the subscript \* denotes the complex conjugate. The latter coefficients are calculated according to Born & Wolf (1980) as

$$\tilde{R}_{1,2} = \frac{(\varphi_0^2 - 2\delta_1 + i2\beta_1)^{1/2} - (\varphi_0^2 - 2\delta_2 + i2\beta_2)^{1/2}}{(\varphi_0^2 - 2\delta_1 + i2\beta_1)^{1/2} + (\varphi_0^2 - 2\delta_2 + i2\beta_2)^{1/2}}.$$

With this we can write  $t(l) = \exp(-|l/L|)R^n$ . Here  $L$  is the attenuation length of the core material, which is tabulated (Henke *et al.*, 1993; Chantler *et al.*, 2003). Now we will ignore the integer character of  $n$  and substitute it with a continuously varying number  $n(l) = |l/\Delta l|$ , where  $\Delta l$  is the longitudinal beam advance between two consecutive bounces in the waveguide resonator  $\Delta l \simeq D_{\text{eff}}/\varphi_2$ . In addition we will use the reflectivity decrement  $\Delta R$ , which in  $R = 1 - \Delta R$  is assumed to satisfy  $\Delta R \ll 1$ . So one can write  $R^{n(l)} = \exp(-|l/\Delta l| \Delta R)$  and thus

$$t(l) = \exp\{-|l|[(1/L) + (\Delta R/\Delta l)]\}. \quad (10)$$

The effective footprint length and the effective aperture are then

$$l_{\text{eff}} = \int_{l_1=-\infty}^{l_2=0} t(l) dl = \frac{1}{[(1/L) + (\Delta R/\Delta l)]} \quad (11)$$

and

$$A_{\text{eff}} = \varphi_0 / [(1/L) + (\Delta R/\Delta l)]. \quad (12)$$

The FWHM footprint size, which will lead to 76% of the effective footprint size  $l_{\text{eff}}$ , instead is realised for  $l_1 = \ln(1 - 0.76)l_{\text{eff}}$ . Consequently

$$l_{\text{FWHM}} = l_2 - l_1 = 1.43l_{\text{eff}} \quad \text{and} \quad A_{\text{FWHM}} = 1.43A_{\text{eff}}. \quad (13)$$

$A_{\text{FWHM}}$  is a geometrical aperture and will be referred to as the FWHM spatial acceptance.

The maximum output flux expected from a waveguide is obtained by multiplying the effective aperture from (12) with the incident photon density and with the coupling efficiency  $\eta$ . The same parameter can also be obtained from rigorous calculations (Parratt, 1954) by integrating the intensity of the standing wavefield over the waveguide core thickness. From a systematic comparison between calculations with the rigorous approach and the presented simple model we find  $\eta = 1$  for  $D_{\text{eff}} > D_{\text{min}}$  and as long as  $4\Delta l \geq L$  for waveguides with low- $Z$  cores enclosed between high- $Z$  cladding layers of optimum thickness. For  $4\Delta l < L$  the coupling becomes inefficient, *i.e.*  $\eta < 1$ . This condition thus sets a practically useful upper limit for the optimum waveguide core thickness at  $D_{\text{max}} = 0.35(\lambda L)^{1/2}$ . The corresponding thickness for the here-discussed low- $Z$  elements, *i.e.* for beryllium PMMA (polymethylmethacrylate,  $\text{C}_5\text{H}_8\text{O}_2$ , density  $1.19 \text{ g cm}^{-3}$ ) and for carbon are  $D_{\text{max,Be}} = 440 \text{ nm}$  at  $E = 17 \text{ keV}$ ,  $D_{\text{max,PMMA}} = 375 \text{ nm}$  at  $E = 32 \text{ keV}$  and  $D_{\text{max,C}} = 300 \text{ nm}$  at  $E = 28 \text{ keV}$ , respectively. Consequently the optimum operation range of X-ray slab waveguides is the submicrometre range.

The angular acceptance  $\Delta\varphi_{\text{FWHM}}$  can readily be calculated from (13) and (5) and is found to be in perfect agreement with the rigorous calculations. If we now consider the number of bounces in the FWHM footprint size  $n_{\text{FWHM}} = l_{\text{FWHM}}/\Delta l$ , then the waveguide angular acceptance is related to it *via*

$$\Delta\varphi_{\text{FWHM}} \simeq \frac{0.88}{n_{\text{FWHM}}} \frac{\varphi_2^2}{\varphi_0}. \quad (14)$$

**2.2.2. Two-dimensional channel waveguides.** In a two-dimensional waveguide the guided modes are bouncing simultaneously between the horizontal and the vertical interfaces. Consequently the transmission function from (10) receives an additional reflectivity term such that the effective footprint length from (11) now reads

$$l_{\text{eff}} = \int_{l_2=-\infty}^{l_1=0} \exp\{-|l|[(1/L) + (\Delta R_v/\Delta l_v) + (\Delta R_h/\Delta l_h)]\} dl \\ = 1/[(1/L) + (\Delta R_v/\Delta l_v) + (\Delta R_h/\Delta l_h)]. \quad (15)$$

The indices now refer to the confinement directions vertical (v) and horizontal (h). Obviously they also need to be added to  $D_{\text{eff}}$ ,  $n_{\text{eff}}$ ,  $\varphi_0$  and  $\varphi_2$  as well as to the effective apertures  $A_{\text{eff}}$  in (12), the spatial acceptances  $A_{\text{FWHM}}$  in (13) and the angular acceptances  $\Delta\varphi_{\text{FWHM}}$  in (14).

## 3. Discussion

The consequences of the above-reported findings for the application of slab waveguides will now be discussed for possible low- $Z$  core materials with one exception. Kovalenko & Chernov (2000) optimized, produced and tested C/Be/C waveguides successfully. In this case the Be/C interfaces have particularly high reflectivity owing to the low absorption in both the Be core and the C cladding layers. However, this combination will not be further discussed here, as it is

the only example in which the phase-space acceptance in all conditions is significantly smaller than that given in (2).

Fig. 2 reports the calculated parameters as they depend on the effective core thickness  $D_{\text{eff}}$  for the most used photon energy of 13 keV. Fig. 2(a) presents the FWHM spatial acceptance  $A_{\text{FWHM}}$  according to (13) and Fig. 2(b) presents the related angular acceptance. The data are presented for  $20 \text{ nm} \leq D_{\text{eff}} \leq 300 \text{ nm}$ , which is the plausible operation range for X-ray waveguides, and for the already tested Mo/Be and Cr/C combinations (Jark *et al.*, 2001). Also in Fig. 2(a) the FWHM spatial acceptance  $A_{\text{FWHM}}$  for waveguides with interchanged core layers are shown.

By comparing the four curves of Fig. 2(a) we see that at larger effective core thickness  $D_{\text{eff}}$  the FWHM spatial acceptance is saturating at values which are determined by the absorption in the core material. At smaller effective core thicknesses the FWHM spatial acceptance is dominated by the reflection losses, which depend more on the cover than on the core material. Note that the initial dependence for all material combinations is found to be approximately  $A_{\text{FWHM}} \propto D_{\text{eff}}^3$ . This is also found at other photon energies and thus the curves always have the same shape. Consequently the curve position in a plot for another photon energy can be obtained from only two calculations at the two extremes for  $D_{\text{eff}}$ .

As all four presented material combinations have identical phase-space acceptance, the material choice does not need to be driven by the request for lowest possible absorption in the guiding layer. Instead, for practical applications one has to consider that optimum performance will require a radiation beam to fill or to overfill both, the spatial and the angular acceptance of the waveguide. Obviously

the small spatial apertures can always be filled. However, this may no longer be the case for the angular acceptance. Indeed, unfocused X-ray beams at state-of-the-art synchrotron radiation sources can have angular spreads even below  $\Delta = 2 \mu\text{rad}$ . Consequently only the angular acceptance of thicker Mo/Be waveguides, as presented in Fig. 2(b) will be filled or overfilled by the incident beam. Instead the angular acceptance of the Cr/C waveguide always remains underfilled, and thus these waveguides provide a smaller output flux. In case a smaller beam from a thinner waveguide is required at the given source, one needs to increase the divergence of the incident beam beyond the waveguide angular acceptance by use of pre-focusing optics. In this case one can opt for the more conveniently producible material combination as the prefocusing can easily be tailored accordingly. Note that in this case the beam divergence needs to be kept such that higher-order modes will not be excited.

At this point we will inspect the FWHM footprint length and spatial acceptance for thicker waveguides operated in the absorption-limited condition. Here we have  $1/L \gg \Delta R/\Delta l$  and  $\varphi_2 \ll \varphi_{c,2}$  and consequently, from (7),  $\varphi_0 \approx \varphi_{c,2}$ . This leads to the upper limits  $l_{\text{FWHM,max}} = 1.43L$  and  $A_{\text{FWHM,max}} = 1.43\varphi_{c,2}L$ . Both exclusively depend on the properties of the core material and on the photon energy. The values calculated by use of the material constants  $L$  and  $\delta$  as tabulated by Chantler *et al.* (2003) are presented in Fig. 3 for the here-discussed low-Z elements. Obviously the ultimate FWHM footprint length  $l_{\text{FWHM,max}}$  is limited to values of the order of 50–60 mm. Consequently, X-ray waveguides can be prepared on conveniently sized mirrors. Significantly shorter mirrors are already sufficient for lower photon energies, for C cores and for thinner waveguides with smaller spatial acceptance. We also see that waveguide spatial apertures are always rather small and are at most about

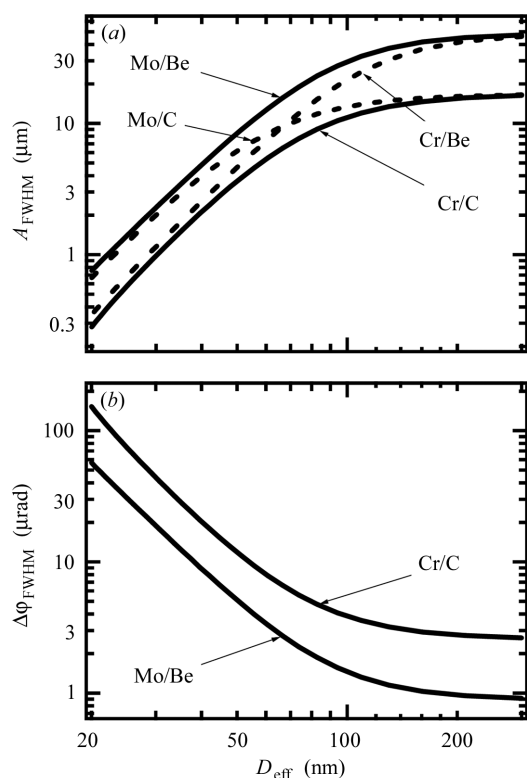


**Figure 2** Acceptance properties for X-ray waveguides depending on effective thickness for the tested material combinations Mo/Be and Cr/C (solid lines) for a photon energy of 13 keV. (a) FWHM spatial acceptances  $A_{\text{FWHM}}$  according to (13) and (b) related angular acceptance  $\Delta\varphi_{\text{FWHM}}$  from (14). The dashed lines in (a) refer to the FWHM spatial acceptances for waveguides with exchanged cores in Mo/C and Cr/Be combinations.

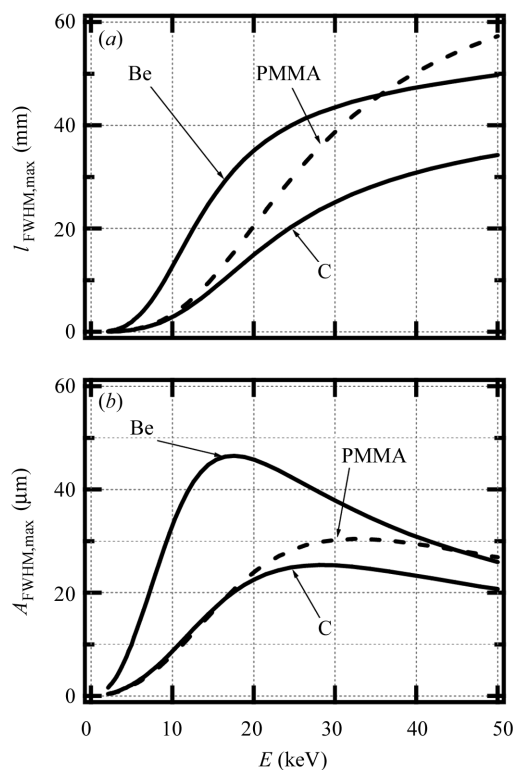


**Figure 3** (a) Upper limit for the FWHM footprint length  $l_{\text{FWHM,max}}$  and (b) related upper limit for the FWHM spatial acceptances  $A_{\text{FWHM,max}}$ , depending on photon energy for possible candidate low-Z materials for the core of waveguides.

47  $\mu\text{m}$  for Be cores and 30  $\mu\text{m}$  for C and PMMA cores. All presented material combinations provide very similar FWHM apertures at photon energies  $>40$  keV. X-ray waveguides could thus be rather promising devices for the latter energy range in which submicrometre foci are not yet reported. Indeed a waveguide with a Be core of thickness  $d_2 = 110$  nm could already compress a 30 keV X-ray beam to below a 100 nm spot size in one dimension (Jark *et al.*, 2001).

4. Interpretation of reported waveguide transmission

Now some previously measured results for X-ray waveguides will be re-examined with the present findings. Usually the experimentally accessible parameter is the transmission of the object as the ratio between the measured flux with optics and without. This parameter is thus extracted appropriately from the reported data.

If the beam aperture  $V$  and beam divergence  $\psi$  fulfill  $V > A_{\text{FWHM}}$  and  $\psi > \Delta\varphi_{\text{FWHM}}$ , the expected transmission for a waveguide is obtained by use of the effective aperture as

$$T = A_{\text{eff}} \Delta\varphi_{\text{FWHM}} / V\psi. \tag{16}$$

The waveguide spatial acceptance is usually significantly overfilled, while the angular acceptance may not be filled completely. In this case, with  $\psi < \Delta\varphi_0$ , one has

$$T(\psi < \Delta\varphi_{\text{FWHM}}) = A_{\text{eff}} / V. \tag{17}$$

These equations can easily be extended for two-dimensional waveguides. Note that the beam aperture needs to be chosen such that it is not spatially coherently illuminated as otherwise the diffraction would increase the beam divergence with a possible subsequent loss in output intensity.

4.1. Transmission of one-dimensional waveguides

Up to now the best performance is reported for one-dimensional waveguides based on Mo/Be (Jark *et al.*, 2001). In this case, two Be cores with two different thicknesses  $d_2 = 74$  nm ( $\text{Be}_1$ ) and  $d_2 = 110$  nm ( $\text{Be}_2$ ) were enclosed between Mo with  $d_1 = 5.5$  nm and  $d_3 = 20$  nm. The fixed  $d_1$  value is optimum for  $\text{Be}_1$  in the photon energy range 13–20 keV, while it is optimum for  $\text{Be}_2$  at 20 keV. Towards smaller photon energies  $d_1$  is always too thick for efficient coupling. From Fig. 2(a) we see that  $\text{Be}_2$  is operated at 13 keV photon energy still in the absorption-limited regime, while for  $\text{Be}_1$  the reflection losses dominate.

Fig. 4 presents a comparison of the measured transmission with the expectations according to (16) or (17). It is notable that both waveguides consistently provide about 50% of the expected transmission at their optimum working energies. It is interesting at this point to calculate the number of bounces  $n_{\text{FWHM}}$  in the FWHM footprint length for the ideal case. For 13 keV photon energy the maximum  $n_{\text{FWHM}} = 79$  is found for  $D_{\text{eff}} = 70$  nm, which is almost the thickness for  $\text{Be}_1$ . At this thickness the performance of  $\text{Be}_1$  is already reflection loss limited and thus the transmission efficiency of 50% requires that part of the exiting radiation undergoes even as many as 40 bounces in the waveguide.

4.2. Transmission of two-dimensional waveguides

The first two-dimensional waveguide was produced by Pfeiffer *et al.* (2002) and was based on a Cr/PMMA combination. It was tested at 12.8 keV photon energy, and thus from the comparison in Fig. 3(b) its properties are expected to be very similar to those of a Cr/C waveguide.

The waveguide had a rectangular core as shown in Fig. 5(a), which was covered on all sides by Cr layers ( $d_{1,v} = d_{1,h} = 6.1$  nm). This layer

thickness is optimum for the realised vertical core thickness of  $d_{2,v} = 62.2$  nm and it is significantly too thick for the horizontal core width  $d_{2,h} = 140.3$  nm. An exiting beam of size 33 nm vertically and 68.7 nm horizontally was observed. The waveguide was positioned at 34 m from the ID13 source at the ESRF with FWHM sizes of  $S_v = 24$   $\mu\text{m}$  and  $S_h = 134$   $\mu\text{m}$  (Cedola *et al.*, 1998). For a beam aperture with  $V_v = 20$   $\mu\text{m}$  and  $V_h = 40$   $\mu\text{m}$  an output photon flux of  $2 \times 10^4$  photons  $\text{s}^{-1}$ , corresponding to an intensity gain of 70, was measured. Consequently the waveguide transmission was  $T = 0.0002$ . Pfeiffer *et al.* (2002) discuss convincingly that the beam was coupled into the structure only through the top cover and not as shown in Fig. 5(a). Then the waveguide horizontal spatial acceptance is identical to the horizontal core width  $A_{\text{eff},h} = d_{2,h} = 0.14$   $\mu\text{m}$ . On the other hand the smaller vertical thickness leads *via* (12) to an effective aperture of  $A_{\text{eff},v} = 4$   $\mu\text{m}$ . Both numbers now result in angular acceptances, which are significantly underfilled by the incident-beam divergence. Note that the vertical aperture  $V_v$  was actually spatially coherently illuminated and thus the beam divergence was increased in it. Nevertheless the waveguide angular acceptance also remained underfilled by the resultant beam divergence.

The expected transmission according to (17) is then simply  $T_{\text{calc}} = A_{\text{eff},v} A_{\text{eff},h} / V_v V_h$ , which gives  $T_{\text{calc}} = 0.0007$ . Consequently the observed transmission of  $T_{\text{exp}} = 0.0002$  corresponds to an experimental waveguide efficiency of  $\eta_{\text{exp}} = T_{\text{exp}} / T_{\text{calc}} = 0.28$ . For each confinement direction this results in an efficiency of  $0.28^{1/2} = 0.53$ , which is essentially identical to the result for the Mo/Be one-dimensional waveguides.

In the present condition the perfect waveguide could thus have provided only 3.6 times higher output flux. Pfeiffer *et al.* (2002) propose the concept shown in Fig. 5(b) in order to couple the beam

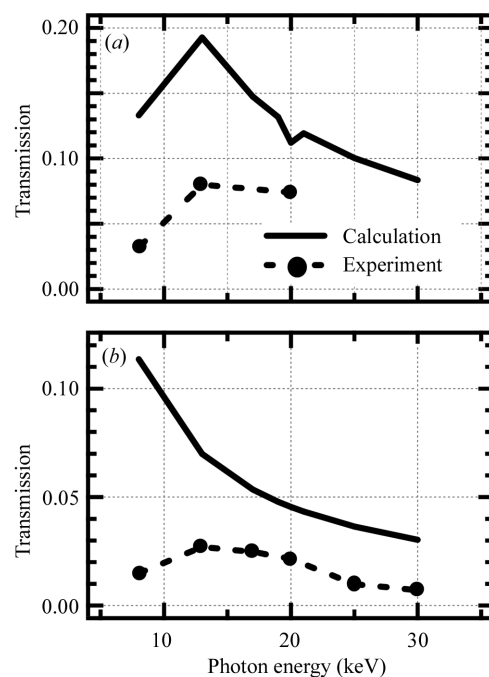
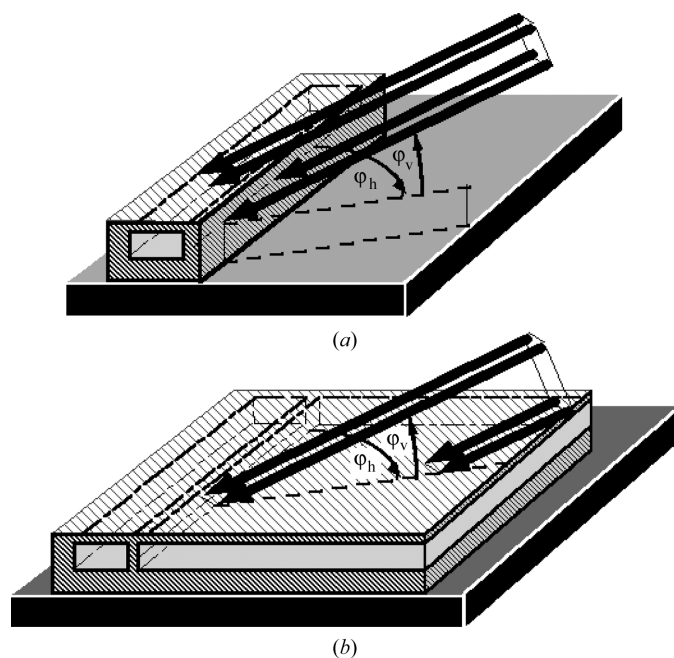


Figure 4 Comparison between the measured waveguide transmission (dots, the dashed line connects the points as a guide for the eye) and the predicted transmission according to (16) or (17) (solid line) depending on photon energy for two waveguides with Be cores sandwiched between Mo layers. The cover layers have thicknesses of  $d_1 = 5.5$  nm, while the core thicknesses are  $d_2 = 74$  nm in (a) and  $d_2 = 110$  nm in (b). The transmission coefficients in (a) and (b) are different as the beam aperture was opened from 50  $\mu\text{m}$  (a) to 100  $\mu\text{m}$  (b).



**Figure 5** Two schemes of possible two-dimensional waveguide concepts [adapted from Pfeiffer *et al.* (2002) and its supplemental material]. In both cases the beam is incident onto the waveguide surface with an angle of grazing incidence  $\varphi_v$ , while the grazing angle of incidence with respect to the vertical waveguide walls is  $\varphi_h$ . (a) Structure for the first successfully tested two-dimensional waveguide with a rectangular PMMA core covered at the top and at the sides with Cr layers. (b) Scheme of a proposed concept for a more efficient two-dimensional waveguide, which has the waveguide core in PMMA separated from an extended PMMA film of identical thickness by a thin vertical Cr wall.

efficiently through the waveguide side wall. Here the incident wave is first vertically confined in a one-dimensional waveguide of thickness identical to the final waveguide channel height. Only subsequently is the horizontal confinement achieved when the guided wave couples at grazing incidence into the system confined on one side with the thin vertical wall. This vertical wall has identical material at both sides so that the refraction will not change the beam properties in this second coupling process. However, the effective aperture in the horizontal direction will increase according to (12) to  $A_{\text{eff,h}} = 0.7 \mu\text{m}$ , *i.e.* only about fivefold, while the angular acceptance remains underfilled. Consequently the latter waveguide can only be used efficiently if the divergence of the incident beam is better matched in both directions to the waveguide angular acceptances by an additional optics.

**5. Conclusion**

It is shown that the spatial acceptance for an X-ray waveguide can be calculated from plausible arguments. X-ray waveguides filter the spatially coherent part out of the incident radiation beam. This allows one then to derive the angular acceptance from the phase-space volume for spatially coherent radiation. These calculations are consistent with rigorous calculations based on recursion techniques. It is found that the experimental transmission efficiency of state-of-the-art one- and two-dimensional waveguides is 50% for any confinement direction. Consequently the transmission for one-dimensional X-ray waveguides is 50% of the incident spatially coherent radiation, while it is 28% for the first two-dimensional version. It is pointed out that thinner waveguides can provide their optimum performance at state-of-the-art synchrotron radiation

sources only if the beam divergence is eventually increased to the waveguide angular acceptance by use of additional optical components.

We gratefully acknowledge Drs C. Giannini and L. De Caro of CNR, Bari (Italy) and Drs A. Cedola and S. Lagomarsino of CNR, Rome (Italy), whose interest and questions initiated this study. We thank very much Drs N. V. Kovalenko and V. A. Chernov from the Budker Institute of Nuclear Physics, Novosibirsk (Russia) for many discussions and for the information related to their work on C/Be/C waveguides.

**References**

Andruszkow, J. *et al.* (2000). *Phys. Rev. Lett.* **85**, 3825–3829.  
 Attwood, D. (1999). *Soft X-rays and Extreme Ultraviolet Radiation: Principles and Applications*, ch. 8. Cambridge University Press.  
 Bergemann, C., Keymeulen, H. & van der Veen, J. F. (2003). *Phys. Rev. Lett.* **91**, 204801.  
 Bilderback, D. H., Hoffman, S. A. & Thiel, D. J. (1994). *Science*, **263**, 201–203.  
 Bongaerts, J. H. H., David, C., Drakopoulos, M., Zwanenburg, M. J., Wegdam, G. H., Lackner, T., Keymeulen, H. & van der Veen, J. F. (2002). *J. Synchrotron Rad.* **9**, 383–393.  
 Born, M. & Wolf, E. (1980). *Principle of Optics*, 6th ed. New York: Pergamon Press.  
 Cedola, A., Lagomarsino, S., Di Fonzo, S., Jark, W., Riekel, C. & Deschamps, P. (1998). *J. Synchrotron Rad.* **5**, 17–22.  
 Chantler, C. T., Olsen, K., Dragoset, R. A., Kishore, A. R., Kotochigova, S. A. & Zucker, D. S. (2003). *X-ray Form Factor, Attenuation and Scattering Tables (Version 2.0)*, <http://physics.nist.gov/ffast>. [Originally published as Chantler, C. T. (2000). *J. Phys. Chem. Ref. Data*, **29**, 597–1048 and Chantler, C. T. (1995). *J. Phys. Chem. Ref. Data*, **24**, 71–643.]  
 Chao, W., Anderson, E., Denbeaux, G. P., Harteneck, B., Liddle, J. A., Olynick, D. L., Pearson, A. L., Salmassi, F., Song, C. Y. & Attwood, D. T. (2003). *Opt. Lett.* **28**, 2019–2021.  
 De Caro, L., Giannini, C., Di Fonzo, S., Jark, W., Cedola, A. & Lagomarsino, S. (2003). *Opt. Commun.* **217**, 31–45.  
 Di Fabrizio, E., Romanato, F., Gentili, M., Cabrini, S., Kaulich, B., Susini, J. & Barrett, R. (1999). *Nature (London)*, **401**, 895–898.  
 Di Fonzo, S., Jark, W., Lagomarsino, S., Giannini, C., De Caro, L., Cedola, A. & Müller, M. (2000). *Nature (London)*, **403**, 638–640.  
 Feng, Y. P., Sinha, S. K., Fullerton, E. E., Grübel, G., Abernathy, D., Siddons, D. P. & Hastings, J. B. (1995). *Appl. Phys. Lett.* **67**, 3647–3649.  
 Henke, B. L., Gullickson, E. M. & Davis, J. C. (1993). *Atom. Data Nucl. Data Tables*, **54**, 181–342. [[http://www-cxro.lbl.gov/optical\\_constants/](http://www-cxro.lbl.gov/optical_constants/)]  
 Hignette, O. (2003). Private communication.  
 Jark, W. (2004). *X-ray Spectrosc.* In the press.  
 Jark, W., Cedola, A., Di Fonzo, S., Fiordelisi, M., Lagomarsino, S., Kovalenko, N. V. & Chernov, V. A. (2001). *Appl. Phys. Lett.* **78**, 1192–1194.  
 Jark, W., Di Fonzo, S., Lagomarsino, S., Cedola, A., di Fabrizio, E., Bram, A. & Riekel, C. (1996). *J. Appl. Phys.* **80**, 4831–4836.  
 Kirkpatrick, P. & Baez, A. (1948). *J. Opt. Soc. Am.* **38**, 766–774.  
 Kovalenko, N. V. & Chernov, V. A. (2000). Private communication.  
 Lagomarsino, S., Cedola, A., Di Fonzo, S., Jark, W., Mocella, V., Pelka, J. B. & Riekel, C. (2002). *Cryst. Res. Technol.* **37**, 758–769.  
 Lagomarsino, S., Jark, W., Di Fonzo, S., Cedola, A., Müller, B. R., Riekel, C. & Engstrom, P. (1996). *J. Appl. Phys.* **79**, 4471–4473.  
 Lengeler, B., Schroer, C. G., Tuemmler, J., Benner, B., Richwin, M., Snigirev, A., Snigireva, I. & Drakopoulos, M. (1999). *J. Synchrotron Rad.* **6**, 1153–1167.  
 Marcuse, D. (1991). *Theory of Dielectric Waveguides*. San Diego: Academic Press.  
 Parratt, L. G. (1954). *Phys. Rev.* **95**, 395–402.  
 Pfeiffer, F. (1999). Diploma thesis, Ludwig-Maximilians-Universität München, Germany. [See also Pfeiffer, F., Salditt, T., Høghøj, P., Anderson, I. & Schell, N. (2000). *Phys. Rev. B*, **62**, 16939–16943.]  
 Pfeiffer, F., David, C., Burghammer, M., Riekel, C. & Salditt, T. (2002). *Science*, **297**, 230–234. [<http://www.sciencemag.org/cgi/data/297/5579/230/DC1/1>]  
 Schmahl, G. & Rudolph, D. (1969). *Optik*, **29**, 577–585.

- Schroer, C. G., Kuhlmann, M., Hunger, U. T., Günzler, T. F., Kurapova, O., Feste, S., Frehse, F., Lengeler, B., Drakopoulos, M., Somogyi, A., Simionovici, A. S., Snigirev A., Snigireva, I. & Schug, C. (2003). *Appl. Phys. Lett.* **82**, 1485–1487.
- Snigirev, A., Kohn, V., Snigireva, I. & Lengeler, B. (1996). *Nature (London)*, **384**, 49–51.
- Spiller, E. & Segmüller, A. (1974). *Appl. Phys. Lett.* **24**, 60–61.
- Yun, W., Lai, B., Cai, Z., Maser, J., Legnini, D., Gluskin, E., Chen, Z., Krasnoperova, A. A., Vladimirovsky, Y., Cerrina, F., Di Fabrizio, E. & Gentili, M. (1999). *Rev. Sci. Instrum.* **70**, 3537–3541.
- Zwanenburg, M. J., Bongaerts, J. H. H., Peters, J. F., Riese, D. & van der Veen, J. F. (2000). *Physica B*, **283**, 285–288.
- Zwanenburg, M. J., Peters, J. F., Bongaerts, J. H. H., de Vries, S. A., Abernathy, D. L. & van der Veen, J. F. (1999). *Phys. Rev. Lett.* **82**, 1696–1699.